SSC-N-537
3 August 1988

DIPOLE SYSTEM REQUIREMENTS: LIFETIME RADIATION DOSES AND NEUTRON FLUENCES IN THE SSC ARCS

D. E. Groom
3 August 1988

A fair amount of effort has gone into understanding the radiation environment in parts of the machine where continuous beam losses (e.g. due to beam-gas collisions) are expected to be the main source of radiation. At this stage the conclusions are not as detailed, coherent, or trustworthy as one might wish, but there is reasonable consistency and results probably will not change by factors of more than two.

The present status is summarized on the third page. Following is an annotated list of references on the subject, the most important of which are appended.

1. D. E. Groom, "Radiation in the SSC Main Ring Tunnel," Appendix 21 of "Report of the Task Force on Radiation Effects at the SSC," M. G. D. Gilchriese, Editor, SSC Central Design Group Report SSC-SR-1035 (1988). This appendix summarizes most of the available information. *Copy attached.*
2. T. A. Gabriel, F. S. Alsmiller, R. G. Alsmiller, Jr., B. L. Bishop, O. W. Hermann, and D. E. Groom, "Preliminary Simulations of the Neutron Flux Levels in the Fermilab Tunnel and Proposed SSC Tunnel," SSC Central Design Group Report SSC-110 (1987).
3. D. E. Groom, "Measurements and Simulations of the Neutron Flux in the Tevatron Tunnel," Appendix 10 of "Report of the Task Force on Radiation Levels in the SSC Interaction Regions," D. E. Groom, Editor, SSC Central Design Group Report SSC-SR-1033 (1988). Reference 2 is summarized. *Copy attached.*
4. D. E. Groom, "Ionizing Radiation Dose in the SSC Dipole Magnet Correction Coils," SSC Central Design Group Report SSC-N-439 (08 January 1988). *Copy attached.*
5. N. V. Mokhov, "Energy Deposition and Particle Fluence Distribution in the SSC Dipole Magnet and in the Tunnel under Beam Losses in the Regular Arc Cells," Appendix 22 of "Report of the Task Force on Radiation Effects at the SSC," M. G. D. Gilchriese, Editor, SSC Central Design Group Report SSC-SR-1035 (1988). Mokhov's calculations are independent of those

summarized in Refs. 3 and 4, and as such provide valuable corroboration. The ionizing doses are within a factor of two of Fassò's (Ref. 4.) *Copy attached.*

6. H. Schönbacher and F. Coninckx, "Doses to the SpS from 1976 to 1986 and Estimate of Radiation Damage," Appendix 23 of "Report of the Task Force on Radiation Effects at the SSC," M. G. D. Gilchriese, Editor, SSC Central Design Group Report SSC-SR-1035 (1988). This thorough analysis of experience at the SpS indicates that excursions in dose rate may exceed averages because actual losses are far from uniform.
7. M. G. D. Gilchriese, "Maximum Radiation Levels in Magnet Coils from Point Losses," Appendix 24 of "Report of the Task Force on Radiation Effects at the SSC," M. G. D. Gilchriese, Editor, SSC Central Design Group Report SSC-SR-1035 (1988). *Copy attached.*

SUMMARY: Radiation in the SSC arcs

Assumptions:

- 4×10^{14} protons per ring for 10^7 seconds/year
- Distributed losses corresponding to $(300\ \text{hr})^{-1}$ contribution to reciprocal of current lifetime
- 30 year machine lifetime

$\Longrightarrow$ Loss of 1.3×10^{12} protons per meter

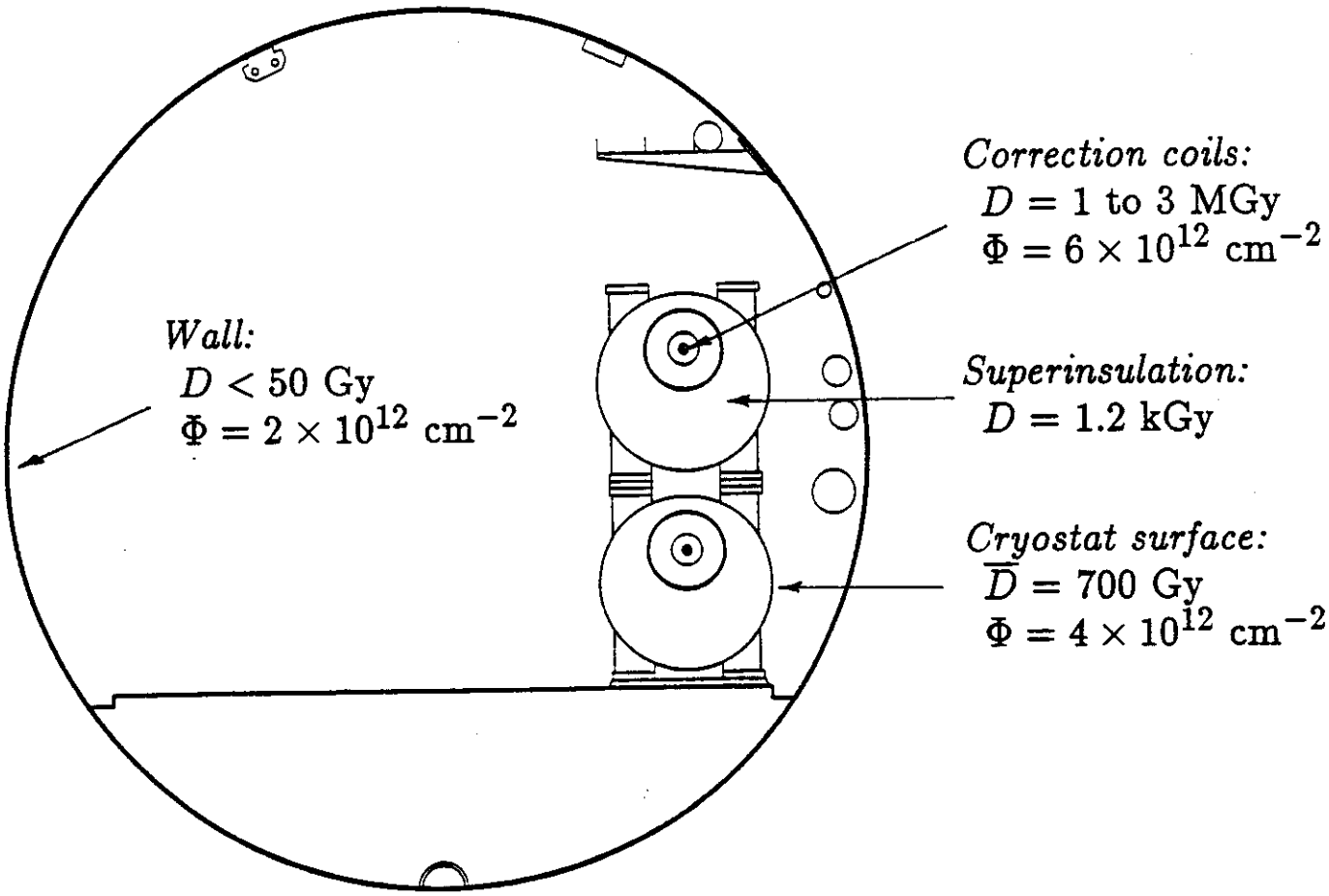

Comment: Doses at cryostat wall and at tunnel wall are not consistent. On basis of cryostat figure, dose of 100 Gy is expected at tunnel wall.

APPENDIX 21*

RADIATION IN THE SSC MAIN RING TUNNEL

D. E. Groom

SSC Central Design Group, LBL90-4040, Berkeley CA 94720

1. Introduction

Estimates of the ionizing dose rate and neutron flux in the SSC arcs have been made, based upon neutron flux simulations by the Oak Ridge group [1], measurements of the neutron flux in the Tevatron tunnel [2, 3], and dose simulations by Fasso [4]. We summarize them here under a set of consistent assumptions about machine operation, with the warning that all are preliminary and that some have not yet been checked adequately.

N. Mokhov and his collaborators have made totally independent calculations using the MARS10 code. Their results, published as a separate Appendix to this Report, provide welcome corraboration.

2. Assumptions

Since these estimates are to be used in estimating component and materials lifetimes, it seems prudent to make "worst case" assumptions with regard to beam current and loss rate. We therefore assume that each ring contains 4×10^{14} protons for 10^7 seconds of each year. Although distributed particle loss depends upon factors which are not well understood, we assume that these processes (beam-gas collisions, etc.) contribute 300 h to the beam current lifetime, for a loss rate of 3.7×10^8 s^{-1}, or 3.7×10^{15} per year. Since the ring is 85 km in circumference, this loss rate corresponds to 44 $cm^{-1}s^{-1}$. Annual fluences and doses are quoted; the reader may multiply by 30 years to obtain estimates over the lifetime of the machine. The beam energy is 20 TeV.

Quoted neutron fluences are for neutron kinetic energies above 40 keV; for the expected spectra (see below) this is about the same as the fluence above 100 keV.

3. Neutron fluence near the tunnel wall (distributed loss)

In SSC-110, it is concluded that the flux near the SSC tunnel wall (2 m from the magnets) for one ring only is

$$\phi = 2900\ N_{14} C_{83}^{-1} \tau_{100}^{-1}\ \mathrm{cm}^{-2}\mathrm{s}^{-1}$$

where N_{14} is the number of protons in the ring in units of 10^{14} and the other

* Appendix 21 from "Report of the Task Force on Radiation Effects at the SSC," M. G. D. Gilchriese, Editor, SSC Central Design Group Report SSC-SR-1035 (1988).

scaled variables refer to an 83 km circumference and a 100 hour lifetime. Our present assumptions are $N_{14} = 4$, $C_{83} = 1.02$, and $\tau_{100} = 3$, so that the expected flux is 3800 $\mathrm{cm^{-2}s^{-1}}$ per ring, or 7600 $\mathrm{cm^{-2}s^{-1}}$ for both rings. The annual fluence is then 8×10^{10} $\mathrm{cm^{-2}s^{-1}}$.

This number is corroborated by measurements in the Tevatron tunnel under stored beam conditions, with cascades initiated by collisions with nitrogen from a controlled leak. The agreement between experiment and simulation is better than a factor of two. Most of the uncertainty is experimental, because of a poorly known pressure gauge calibration. The simulation indicates that the flux scales with beam energy as $E^{0.8}$, in agreement with expectation.

The spectrum is dominated by a peak just under 1 MeV which is roughly gaussian in $\ln E$:

$$\frac{d\varphi}{d(\ln E)} \propto \mathrm{e}^{-\ln(E/E_0)/\sigma} ,$$

where $E_0 \approx 0.55$ MeV and $\sigma \approx 1.3$. Most of the integral under this peak is above 0.1 MeV, and there is very little above 10 MeV. The spectrum again rises at low energies. It is not as well determined in this region, but the area corresponding to thermal energies is about equal to that under the 1 MeV peak.

4. Neutron fluence near and inside the magnets (distributed loss).

According to the simulation results, 80% of the flux at the tunnel wall (200 cm from the magnets) is due to neutrons which have been reflected at least once from the concrete walls. The direct flux should scale as the reciprocal of the distance from the magnet string, while the reflected component should be more or less independent of position. Let φ_w be the flux at the wall due to both rings, and let f be the fraction of the flux which has been reflected (0.8 in this case). The the flux anywhere outside a magnet yoke is

$$\begin{aligned}
\varphi &= \tfrac{1}{2}\varphi_w \left[f + (1-f)\left(\frac{200\ \mathrm{cm}}{r_1}\right) \right. \\
&\qquad \left. + f + (1-f)\left(\frac{200\ \mathrm{cm}}{r_2}\right) \right] \\
&= \varphi_w \left[f + \left(\frac{1-f}{2}\right)\left(\frac{200\ \mathrm{cm}}{r_1} + \frac{200\ \mathrm{cm}}{r_2}\right) \right] \\
&= 7600\ \mathrm{cm^{-2}s^{-1}} \left[0.8 + 0.1\left(\frac{200\ \mathrm{cm}}{r_1} + \frac{200\ \mathrm{cm}}{r_2}\right) \right]
\end{aligned}$$

where r_1 and r_2 are the distance from the observation point to the centers of the beam lines. The yoke itself has a radius of 13 cm. Since this distance is

comparable to the scattering length of 1 MeV neutrons in iron, the neutron flux inside it should be fairly uniform. We therefore use the flux at the surface as an estimator of the flux inside.

On the surface of a cryostat, $r_1 \approx 30$ cm and $r_1 \approx 70$ cm, so the enhancement factor in the square brackets is 1.8. Inside the iron we take $r_1 \approx 13$ cm and obtain an enhancement factor of 2.6. The corresponding annual fluences are 1.3×10^{11} cm^{-2} at the surface of the cryostat and 2×10^{11} cm^{-2} inside the yoke.

5. Maximum neutron fluence near a loss point

According to Fig. 5 of SSC-110, a maximum neutron flux at the tunnel wall of 0.1 neutrons cm^{-2} occurs about 6 m downstream of the interaction point. Fig. 4 of the report, which shows the same distributions at 875 GeV, suggests that the experimental distribution is flatter than the simulation would suggest. In addition, the configuration of both the simulation and measurements is somewhat different than for a continuous dipole string. However, 0.1 cm^{-2} per interacting proton is sufficiently accurate for our present purposes.

If 10^{-6} of the protons are lost once per day 100 days of the year, the annual fluence just downstream of the loss point will be 4×10^9 cm^{-2}. This is 1/20 of the fluence estimated for distributed losses. A loss of 10^{-4} of the beam once per day at a scraper, septum, or other special location will thus produce a much greater fluence than continuous processes.

6. Dose in the tunnel (distributed loss)

Limits on the ratio of ionizing dose rate to neutron flux in the Tevatron tunnel are reported in SSC-58. Their reported limits for ionizing particles and photons can be combined to obtain

$$D/\varphi < 2 \times 10^{-11} \text{ Gy cm}^2 .$$

We may assume that the ratio is the same for the SSC; then the annual dose near the wall is less than 1.5 Gy.

7. Maximum dose near the inside of the superconducting coils

Preliminary dose calculations by Alberto Fassò are reported in SSC-N-439. He finds that

(a) the maximum dose occurs in the central plane in the smallest radial bin, corresponding to the beam pipe, correction coil, or inner edge of the main superconducting winding.

(b) in the longitudinal direction the maximum dose occurs about 30 cm downstream of the primary collision point, where it reaches about 50 GeV

cm^{-3}per incident particle. The average over the next meter is between 20 GeV cm^{-3} and 30 GeV cm^{-3}.

(c) the longitudinal integral for the inner bin is 3650 GeV cm^{-2}.

The integral implies $3650/(85 \times 10^5)$ GeV cm^{-3} at a point if the loss is averaged around the ring, or 1.6×10^{12} GeV cm^{-3} yr^{-1} for our assumed loss rate. Multiplying by 1.6×10^{-10} J GeV^{-1} and dividing by the density, 0.007 kg cm^{-3}, we obtain an annual dose of 3.6×10^4 Gy.

If 10^{-6} of the beam is lost 100 times per year at a given point, the maximum dose downstream may be obtained using 50 GeV cm^{-3} per lost particle, or 5×10^4 Gy yr^{-1}. Since losses occur over at least a meter because of the finite beam width and grazing angle of incidence, it is appropriate to somewhat derate this number, e.g. to 2×10^4 Gy yr^{-1}. In any case, a local loss of 10^{-6} per day 100 times a year is as serious as the expected distributed loss.

Table 1
Ionizing radiation dose and neutron fluence in the SSC tunnel

	Annual dose or fluence
1. Average around the ring	
Maximum dose in dipole coil	3.6×10^4 Gy
Dose in tunnel (at wall)	< 1.5 Gy
Neutron fluence in tunnel (at wall)	8×10^{10} cm^{-2}
Neutron fluence at cryostat	1.3×10^{11} cm^{-2}
Neutron fluence inside yoke	2×10^{11} cm^{-2}
2. 10^{-6} of one beam lost at a point 100 times per year	
Maximum dose in dipole coil	2×10^4 Gy
Maximum neutron fluence at tunnel wall	4×10^9 cm^{-2}

8. Conclusions

The results are summarized in Table 1. The neutron fluences are relatively well known, while the ionizing radiation doses are highly preliminary. The radiation field near a point where beam loss occurs is relatively easily calculated, but expected loss rates are essentially unknown.

9. References

1. T. A. Gabriel, F. S. Alsmiller, R. G. Alsmiller, Jr., B. L. Bishop, O. W. Hermann, and D. E. Groom, "Preliminary Simulations of the Neutron Flux Levels in the Fermilab Tunnel and Proposed SSC Tunnel," SSC Central Design Group Report SSC-110 (1987).
2. J. B. McCaslin, R-K. S. Sun, and W. P. Swanson; J. J. Elwyn, W. S. Freeman, and P. M. Yurista, SSC Central Design Group Report No. SSC-58 (1986).
3. J. D. Cossairt, A. J. Elwyn, W. S. Freeman, H. Jöstlein, C. D. Moore, and P. M. Yurista; J. B. McCaslin, R-K. S. Sun, and W. P. Swanson; and D. E. Groom, SSC Central Design Group Report, in preparation (1988).
4. D. E. Groom, "Ionizing Radiation Dose in the SSC Dipole Magnet Correction Coils," SSC Central Design Group Report SSC-N-439 (08 January 1988).
5. D. E. Groom, "More Preliminary Comments: Neutron Flux in the SSC Arcs and Interaction Regions," SSC Central Design Group Report SSC-N-228 (revised) (1987).
6. Memo from D. E. Groom to P. J. Limon concerning the neutron flux at the diodes (08 September 1987).
7. Memo by M. G. D. Gilchriese concerning maximum radiation levels in magnet coils, (08 March 1988).

APPENDIX 10

MEASUREMENT AND SIMULATION OF THE NEUTRON FLUX IN THE TEVATRON TUNNEL

D. E. Groom
SSC Central Design Group, LBL90-4040, Berkeley CA 94720

1. Introduction

In the fall of 1985, a FNAL/LBL group measured neutron spectra in the Tevatron tunnel [1]. These experiments were refined and extended [2] during the machine cycle which ended in the spring of 1987. Absolute magnitude and longitudinal distributions of the neutron flux were measured downstream (in the proton sense) from a warm section in the beam pipe. A controlled N_2 gas leak was introduced near the center of the warm section, so that by measuring rates as a function of gas pressure, beam-gas rates could be separated from background rates. To help support this experimental effort, detailed simulations of particle cascades in the Fermilab tunnel initialed by hadron-nucleus collisions ($E_p = 875$ GeV) in the center of the warm section were carried out at Oak Ridge National Laboratory (ORNL). A version of HETC [3] was used for high-energy particle transport, and the MORSE code [4] was used to transport the low-energy (≤ 20 MeV) neutrons. The preliminary simulation results have been described in an SSC report [5], along with preliminary experimental results.

Many of the results are relevant to radiation in the collision halls and detectors. These include the neutron yield, scaling with energy, the neutron energy spectrum, and the role of neutron reflection from the tunnel walls. Accordingly, we present a short description of the work here, with emphasis upon these aspects.

2. Motivation

The study was motivated by concern about radiation damage to silicon semiconductors in the SSC tunnel, since about 400 racks of control circuitry are located at 200 m intervals around the ring. In addition, temperature sensors, beam pickups, and quench protection diodes are mounted in or on many of the 10,000 magnets. As can be seen from the first figure in Appendix 17, the effective threshold for silicon dislocation damage is about 160 keV. As will be seen, about half of the neutron flux in the tunnel is in a broad peak near 1 MeV, and most of the rest is thermal. Simulations of the hadron-induced flux in detector components yield similar spectra.

3. Simulations

A cross section of the "real" Tevatron tunnel [6] is shown in Fig. A10-1, and the cylindrical approximation used for the simulations is shown in Fig. A10-2.

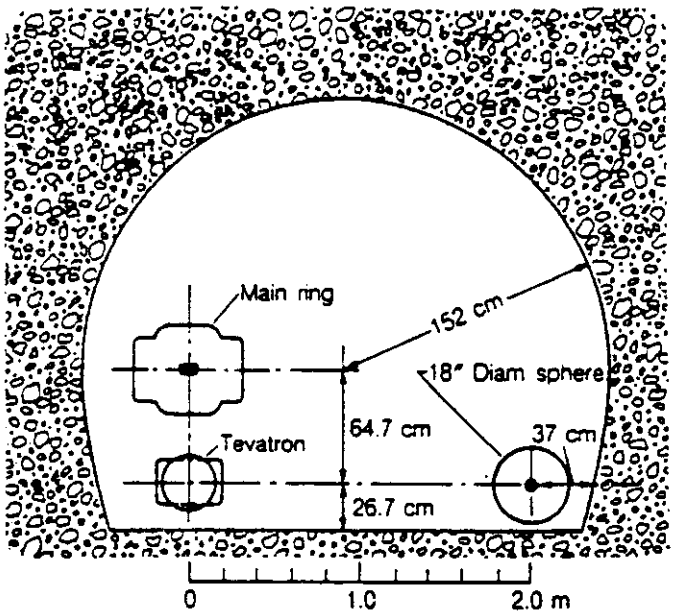

FIG. A10-1. Cross section of the Tevatron tunnel, showing relevant dimensions and the placement of the neutron flux measuring equipment.

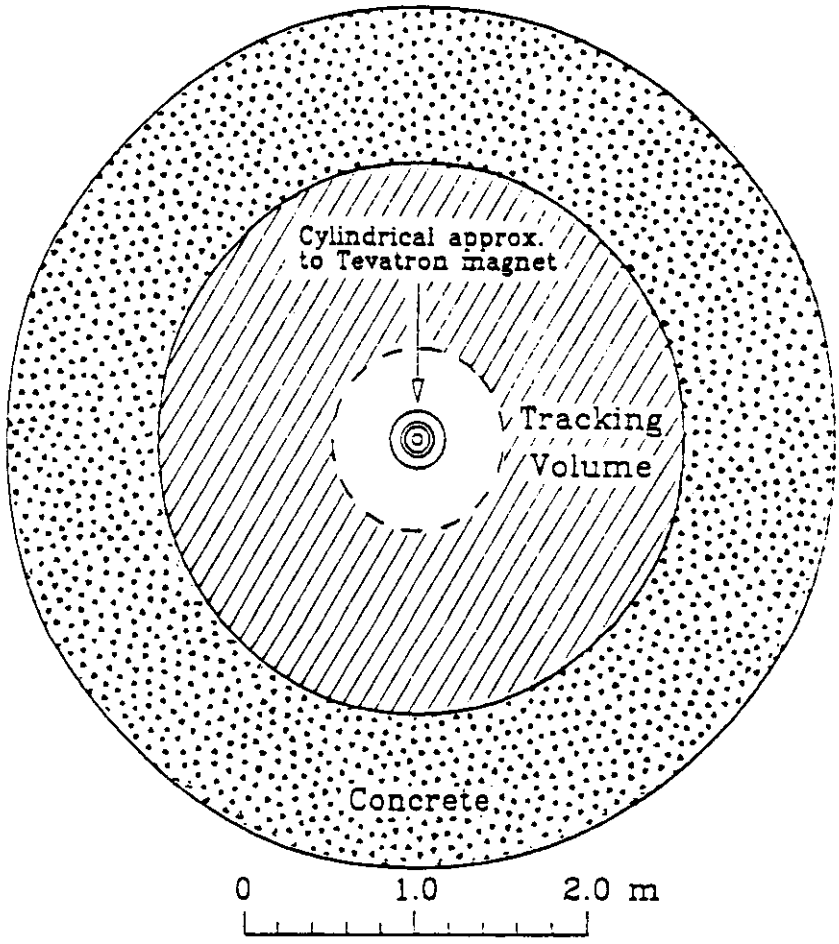

FIG. A10-2. Cross section of the ORNL model to the same scale as Fig. A10-1. Flux is obtained from neutron path lengths scored in the "tracking volume."

The tunnel has the same radius, and the cylindrical approximation to the Tevatron magnet has the same bore area and yoke area as the real one. The correct Tevatron dipole field was used for the 875 GeV simulations, and it was simply raised by 20/0.875 for the 20 TeV simulations. Sagitta was ignored. This approximation leads to problems with the longitudinal flux distribution, and it will be removed for the final version. Similarly, the large scoring volume precludes obtaining radial information about the flux, and finer radial segmentation is now being included.

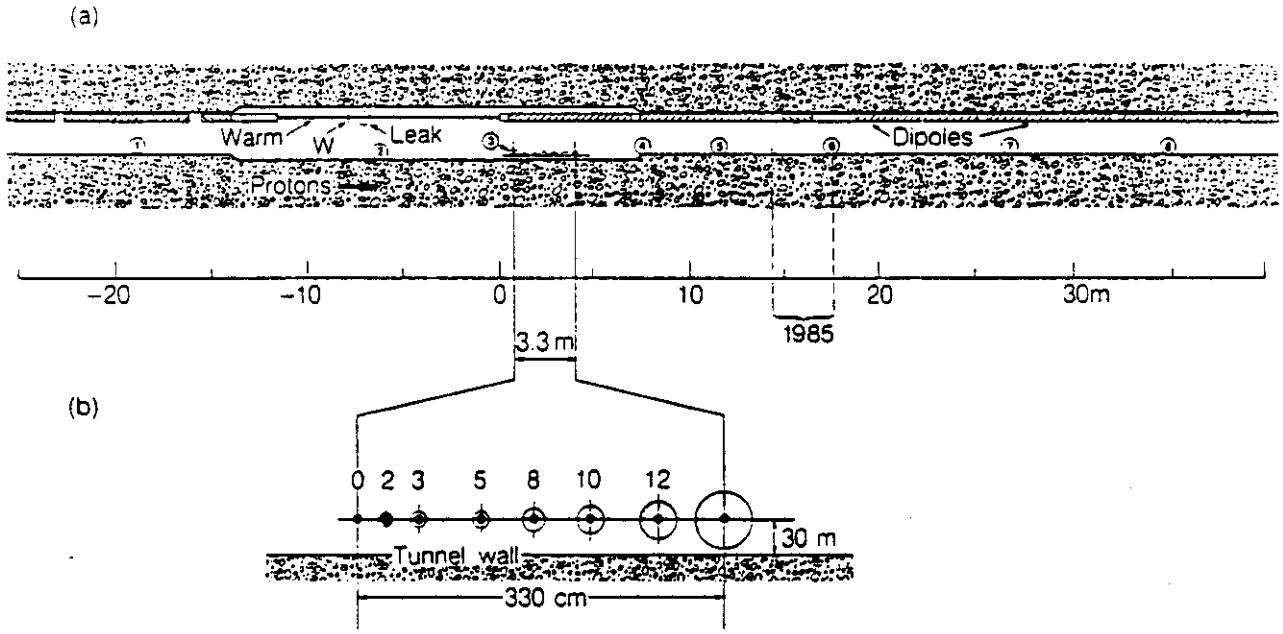

FIG. A10-3. Plan view of experimental setup in the Tevatron tunnel near the A17 straight section. Proton direction is left to right. Nitrogen was allowed to leak into the warm straight section at the point indicated, and the pressure was effectively zero at the cold dipole entrances on either end. Identical Bonner spheres at the numbered locations were used to measure the longitudinal distribution, and the full spectrometer (as shown in the enlargement) was used to obtain the spectrum shown in Fig. A10-4. The effective position of the spectrometer in the 1985 experiment (actually in A48) is marked by "1985."

A plan view of the Tevatron tunnel is shown in Fig. A10-3.

The actual density profile of the N_2 target gas is triangular. Since experiments using a "flying wire" target were also planned, the target was modeled as a thin iron wire in the center of the warm section.

Approximately 3000 neutrons per 875 GeV proton and 30,000 neutrons per 20 TeV proton are produced in HETC for transport in the MORSE code. Fewer than 3% of these low-energy neutrons originate in collisions with hadrons of energy above 3 GeV.

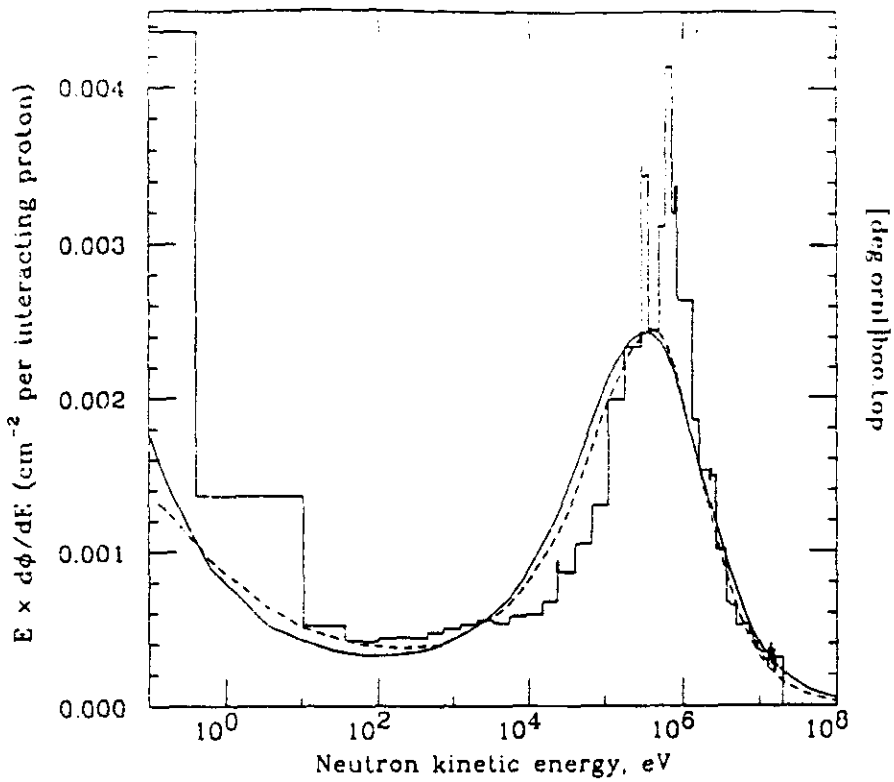

FIG. A10-4. The histogram shows the energy spectrum of the total neutron flux near the maximum of the longitudinal distribution in an 875 GeV simulation. The dotted curve is the result of folding these data with the Bonner sphere responses and then unfolding using the program LOUHI[7]. The solid curve is obtained when the normalized rates from the N_2 gas (slope data) are unfolded with the same program.

It was of interest to understand the role of neutron scattering from the tunnel walls. Accordingly, runs were made with the profile shown in Fig. A10-2 and with the same geometry with the concrete replaced by vacuum ("no tunnel walls"). The "no walls" case yielded the direct flux, and the difference of the two cases yielded the scattered or "albedo" flux. Runs for both cases were made at 875 GeV and 20 TeV.

A typical spectrum is shown by the histogram in Fig. A10-4. When plotted in this way ($d\varphi/d\ln E$ as a function of $\ln E$, where E is the neutron's kinetic energy), about half the flux is in a broad gaussian peak centered at about 600 keV. Since most of the computer time was spent transporting neutrons in the thermal region, most subsequent runs were made with the lower threshold in MORSE set at 40 keV. As can be seen from the figure, a cut at this energy yields about the same integral as does a cut at 160 keV (our effective threshold for silicon damage).

Longitudinal distributions at 875 GeV are shown by the histograms in Fig. A10-5. The total and direct fluxes are obtained directly from the simulations, while the albedo contribution is obtained by subtraction, as discussed above.

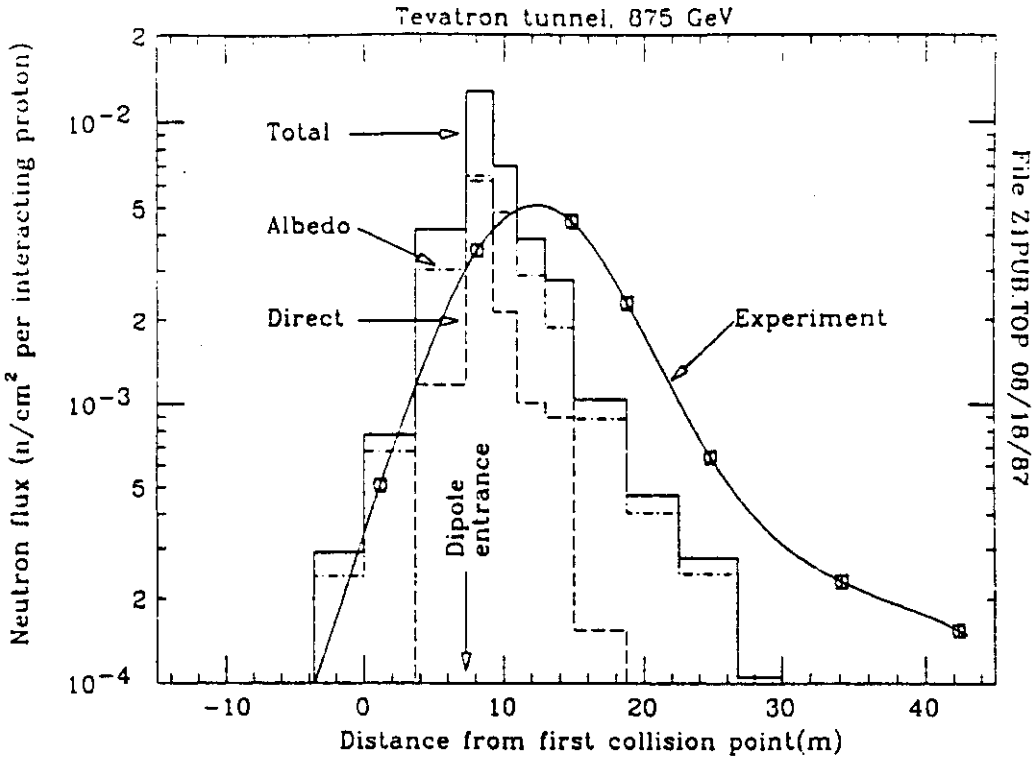

FIG. A10-5. Calculated longitudinal distributions of neutron flux ($E > 40$ keV) in the Tevatron tunnel for 875 GeV incident proton energy (histograms), and measured distribution (symbols connected with spline).

The direct flux is more sharply peaked, since the albedo neutrons have had more opportunity to diffuse along the tunnel.

In addition to a more extended longitudinal distribution, the 20 TeV results show a long, flat tail composed almost entirely of albedo particles.

Suppose that a proton interacts at a point z' with probability dz'/C in a continuous magnet string, as is the case for beam-gas collisions in the SSC. A detector at a point z, at a given distance from the magnet, measures a flux $f(z-z')dz'/C$. The total flux in the detector from uniformly distributed sources of this kind will then be

$$\phi = \frac{1}{C}\int f(z-z')dz'$$
$$= \frac{1}{C}\int f(z')dz'$$

when the integral is carried out over all z' for which f is non-zero. In making the connection between the continuously distributed case and the localized distribution, it is thus the *integral* of the distribution which is relevant. The function $f(z)$ is somewhat different than the longitudinal distribution measured in the Tevatron experiment or calculated in the present simulation, where the source is

Table A10-1
z-integrals of the total neutron flux above 40 keV
as obtained from the December 1986 simulations.

Run	875 GeV ((neutrons cm^{-2})×cm per interacting proton)	20 TeV ((neutrons cm^{-2})×cm per interacting proton)	Ratio
Total	7.70	105.6	13.7
Direct	2.54	35.5	14.0
Albedo*	5.15	70.1	13.6
Albedo + 0.66 Dir.	6.83	93.5	13.7

* Obtained by subtracting the direct flux from the total flux.

in a long field-free region. However, the integral is virtually the same, and it is the z-integrals of the functions shown in Fig. 10-4 which is needed.

The z-integrals of the flux above 40 keV are given in Table A10-1. An upper limit to the ratio of the integrals (the scaling factor with energy) is given by the ratio (20.0 TeV)/(0.875 TeV) = 22.9. The expected value for the scale factor is somewhat lower than this limit; at the higher energies a larger fraction of the cascade is "bled off" into electromagnetic showers because there are more generations of π^0 production. Lindenbaum has suggested that the scaling with energy should be approximately a power law E^m, and the present best value for the exponent is $m = 0.80 \pm 0.10$ [8]. This scaling would predict a ratio of $12.2^{+4.5}_{-3.3}$, in good agreement with the present result.

Let a be the mean number of times a neutron is scattered from the tunnel walls before it is absorbed or loses too much energy to be counted. It is shown in Appendix 9 that the total flux is then enhanced by a factor $(1 + 8ar/\pi R)$, where the point of observation is r from the dipole string and the radius of the tunnel is R. The Tevatron tunnel has a radius of 152 cm. The scoring volume in the simulation is such that r should be replaced by a mean radius $\langle r \rangle = 101$ cm, so that $(1+8ar/\pi R) = (1+1.69a)$. This quantity should be equal to the ratio of the total to direct flux, from which we obtain $a = 1.18$ from the data in the table. At the tunnel wall, $(1 + 8ar/\pi R) = (1 + 2.54a)$. Comparing the two expressions, we see that only 0.66 of the direct flux scored in the simulation would be measured near the tunnel wall. The last row in the table thus contains the Monte Carlo prediction for the longitudinal flux integral.

Simulation spectra near the maximum of the longitudinal distribution are shown in Fig. A9-6. One might have expected the albedo contribution to be considerably softer than the direct part, because of moderation in the hydroge-

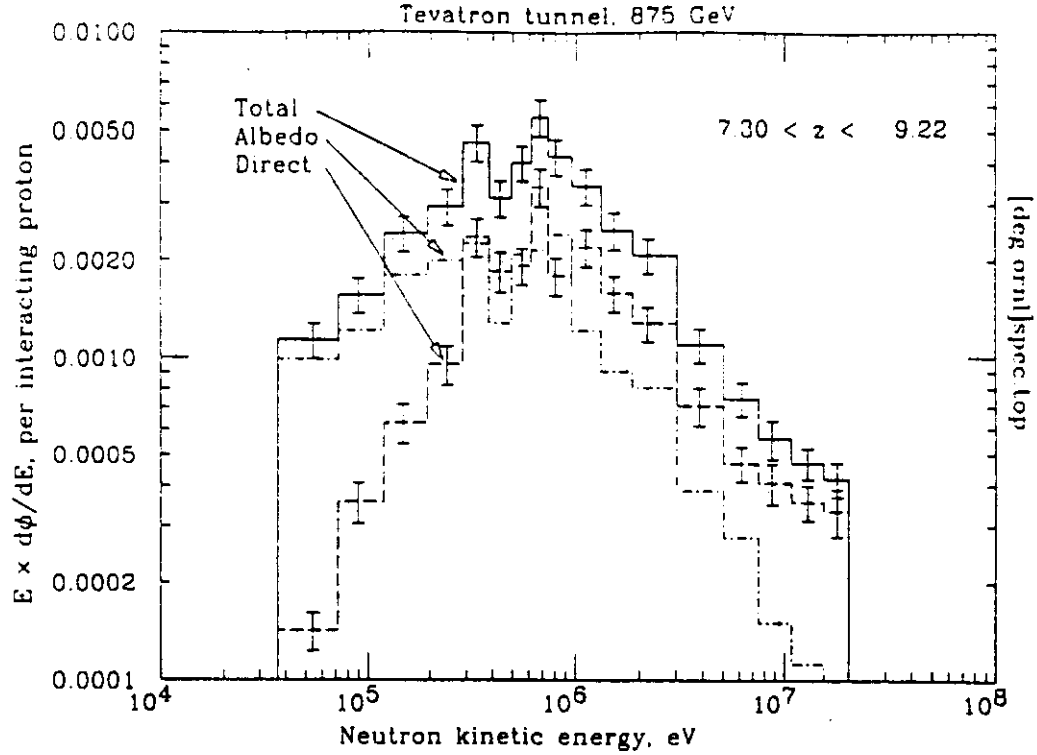

FIG. A10-6. Neutron spectra obtained in the 875 GeV Tevatron tunnel simulations at a longitudinal position near the maximum.

nous walls. This is only slightly true. The main effect is a "fill-in" of the valley between the thermal and 1 MeV peaks.

4. Experiment

Neutrons were counted with "Bonner spheres" [9, 10]. Each consisted of a small ^{6}LiI crystal viewed by a photomultiplier, surrounded by a polyethylene sphere. LiI has about the same properties of NaI, except that it is sensitive to thermal neutrons via the reaction $^6\mathrm{Li} + \mathrm{n} \rightarrow {}^3\mathrm{H} + \alpha$. The 4.8 MeV recoil energy is deposited in the crystal, producing a sharp spectral peak whose area can be measured accurately even in the presence of a large background. A "naked" ^{6}LiI crystal is only sensitive to thermal neutrons. The surrounding polyethylene sphere moderates higher-energy neutrons, so the combination has an energy response dependent upon the size of the sphere. For example, in the Tevatron tunnel environment about 85% of the counts observed with 5-inch diameter spheres were from neutrons with energies in excess of 100 keV—neutrons which could damage silicon. From the relative counting rates obtained using the full compliment of 8 detectors, the incident neutron spectrum could be unfolded in a relatively unambiguous fashion.

The setup is shown in Fig. A10-3. The pressure profile of the "target" gas was triangular, with its peak at the place marked "leak" and zeros at the entrances

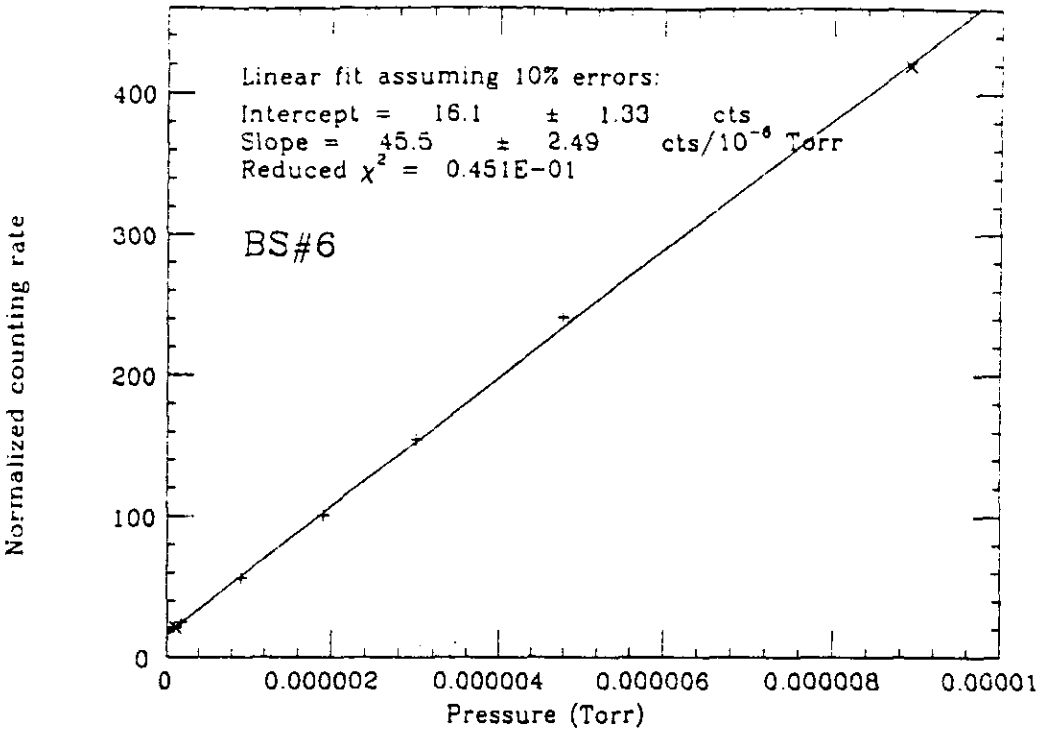

FIG. A10-7. Counting rate versus gauge pressure for a typical Bonner sphere. From the *slope* the rate from a background-free gas target may be extracted, and from the *intercept* the rate from beam loss and other sources not associated with beam-gas interactions in the straight section may be obtained.

to the cold magnets. The longitudinal distribution was measured using identical 5-inch spheres for the reasons stated above. The spectrum was measured with the spheres close together near the flux maximum, as shown in the enlargement. The equivalent position of the spectrometer in 1985 is also shown.

Nitrogen gas leaked into the two-dipole long A17 straight section provided a target of known thickness. Since counting rates scaled linearly with the pressure in the middle of the section, the slope of the pressure-rate relationship yielded the rate change for a know pressure change, and from the intercept the beam-wall and "other" contribution could be extracted. The pressure dependence on gauge pressure for a typical counter is shown in Fig. A10-7. The slopes times some reference pressure were then unfolded using a program such as LOUHI[7] to obtain experimental estimates of the spectra. Such a result is shown by the solid curve in Fig. A10-4. The Monte Carlo and experimental spectra are in rather fortuitous agreement.

The dominant experimental error arises because of the lack of an adequate pressure gauge calibration, but within this error the experimental and simulation rates agreed.

The measured longitudinal distribution of the flux is considerably broader

than that obtained in the simulation. This might be expected for a longitudinally distributed source, but on the other hand most of the collision products should remain within the beam tube until the dipole field is encountered. Further simulations are being made with an extended source and a correctly curving beam tube in an attempt to resolve this question.

Analysis of the experiment is still not complete, but the tentative result is that we should expect an annual neutron fluence of 2×10^{10} neutrons cm^{-2} at the SSC, assuming a 300 hr beam lifetime contribution for distributed losses around the ring [12] and 10^{14} protons in each ring for 10^7 seconds per year. Neutron damage to semiconductors becomes a concern for fluences above 10^{12} cm^{-2}, although carefully chosen components can survive another one or two orders of magnitude more exposure. Given uncertainties about beam loss during injection, the actual beam-gas lifetime, and possible future increases in the proton current, we conclude that the control electronics at alternate spool pieces (every 200 m) should be shielded, either by using the ceiling recesses discussed in the Conceptual Design Report [11] or by placing the shielded electronics racks in niches the side of the main tunnel. Pending the results of further simulations now in progress, we also tentatively conclude that cold diodes inside the cryostats will survive for the life of the machine.

References

1. J. B. McCaslin, R-K. S. Sun, and W. P. Swanson; J. J. Elwyn, W. S. Freeman, and P. M. Yurista, SSC Central Design Group Report No. SSC-58 (1986).
2. J. D. Cossairt, A. J. Elwyn, W. S. Freeman, H. Jöstlein, C. D. Moore, and P. M. Yurista; J. B. McCaslin, R-K. S. Sun, and W. P. Swanson; and D. E. Groom, SSC Central Design Group Report, in preparation (1987).
3. R. G. Alsmiller, Jr. *et al.*, "Modifications of the High Energy Transport Code (HETC) and Comparisons with Experimental Results," presented at the ANS Topical Conference on Theory and Practices in Radiation Protection and Shielding, 22-24 April 1987, Knoxville, Tennessee; K. C. Chandler and T. W. Armstrong, "Operating Instructions for the High-Energy Nucleon-Meson Transport Code HETC," Oak Ridge National Laboratory Report ORNL-4744 (1972)
4. M. B. Emmett, "The MORSE Monte Carlo Radiation Transport Code System," Oak Ridge National Laboratory Report ORNL-4972 (February 1975).
5. T. A. Gabriel, F. S. Alsmiller, R. G. Alsmiller, Jr., B. L. Bishop, O. W. Hermann, and D. E. Groom, "Preliminary Simulations of the Neutron Flux Levels in the Fermilab Tunnel and Proposed SSC Tunnel," SSC Central Design Group Report SSC-110 (1987).
6. H. T. Edwards, *Ann. Rev. Nucl. Part. Sci.* **35**, 605-660 (1985), and F. T. Cole, M. R. Donaldson, D. A. Edwards, H. T. Edwards, and P. F. M. Koehler, editors, "A Report on the Design of the Fermi National Accelerator Laboratory Superconducting Accelerator," Fermilab (1979).
7. J. T. Routti and J. V. Sandberg, "General purpose unfolding program LOUHI 78 with linear and nonlinear regularisations," Compt. Phys. Commun. **21**, 119 (1980).

8. R. H. Thomas and G. R. Stevenson, *Radiological Safety Aspects of the Operation of Proton Accelerators*, IAEA Technical Report Series (1987) (to be published).
9. R. L. Bramblett, R. L. Ewing and T. W. Bonner, Nucl. Instrum. Meth. **9**, 1 (1960).
10. M. Awschalom and R. Sanna, "Applications of Bonner sphere detectors in neutron fields," Rad. Prot. and Dosimetry **10**, 89 (1985).
11. "Superconducting Super Collider Conceptual Design," SSC Central Design Group Report SSC-SR-2020 (1986).
12. D. Bintinger, P. Limon, H. Jöstlein, and D. Trbojevic, "Status of the SSC Photodesorption Experiment," SSC Central Design Group Report SSC-102(1986).